Properties of $CrSi_2$ nanocrystallites grown in a silicon matrix

2007 J. Phys.: Condens. Matter 19 506204

(http://iopscience.iop.org/0953-8984/19/50/506204)

IOP PUBLISHING JOURNAL OF PHYSICS: CONDENSED MATTER

J. Phys.: Condens. Matter **19** (2007) 506204 (13pp) doi:10.1088/0953-8984/19/50/506204

Properties of $CrSi_2$ nanocrystallites grown in a silicon matrix

N G Galkin[1], L Dózsa[2,4], T V Turchin[1], D L Goroshko[1], B Pécz[2], L Tóth[2], L Dobos[2], N Q Khanh[2] and A I Cherednichenko[3]

[1] Institute for Automation and Control Processes of the Far Eastern Branch of the Russian Academy of Sciences, Vladivostok, Russia
[2] Research Institute for Technical Physics and Materials Science, Budapest, Hungary
[3] Institute of Chemistry of FEB RAS, Vladivostok, Russia

E-mail: dozsa@mfa.kfki.hu

Received 17 May 2007, in final form 18 September 2007
Published 19 November 2007
Online at stacks.iop.org/JPhysCM/19/506204

Abstract

Semiconducting $CrSi_2$ nanocrystallites (NCs) were grown by reactive deposition epitaxy. The NCs were covered by 100 nm of epitaxial silicon. Their structure, morphology and optical properties were investigated by transmission electron microscopy (TEM), atomic force microscopy (AFM), ultraviolet photoelectron spectroscopy (UPS) and optical reflectance spectroscopy (ORS). The preservation of the $CrSi_2$ phase has been justified by UPS, by ORS, and by TEM measurements. The distribution of Cr was investigated by Rutherford backscattering (RBS). The electrically active defects were investigated by deep level transient spectroscopy (DLTS). The crystal structure of the NCs nucleated near the deposition depth is identified by high-resolution TEM as hexagonal $CrSi_2$. Energy filtered TEM shows that most of the Cr is localized in the three-dimensional (3D) NCs. RBS shows that the concentration of Cr is appropriate for the deposited quantity. In the 0.1 nm Cr sample most of the Cr is localized near the surface; in the 0.6 nm Cr sample the concentration increases at the depth of Cr deposition, while in the 1.5 nm Cr sample the excess Cr is localized near the deposition depth. DLTS Arrhenius plots give activation energies of the defects appropriate for Cr contamination, however these defects may be related to the $CrSi_2$ NCs.

1. Introduction

Chromium disilicide ($CrSi_2$) is a narrow-band semiconductor ($E_g = 0.35$ eV [1]), which can be epitaxially grown on Si(111) [2]. A strong increase in hole mobility and the decrease in hole concentration have been observed in $CrSi_2$ epitaxial films on Si(111) [3], which corresponds

[4] MTA MFA, Budapest 1525 POB 49, Hungary.

to considerable alterations in their band structure. In a previous study of 0.06–0.12 nm Cr deposition on Si(111), the formation of self-organized semiconductor $CrSi_2$ islands has been observed by differential optical spectroscopy (DOS) and the threshold for 3D nanosize island formation has been determined [4]. The silicon molecular beam epitaxy (MBE) growth atop the $CrSi_2$ nanosize islands was found to be optimal at a temperature of 750 °C and a Si thickness of 50 nm [4]. Using these growth parameters, silicon–silicide heterostructures with multilayers of $CrSi_2$ nanocrystallites (NCs) with 0.6 nm Cr deposition have been grown [4]. The influence of the Cr layer thickness on the formation of Si(111)/$CrSi_2$ NCs/Si(111) heterostructures, their morphology, structure, and optical properties has not yet been studied in the literature.

In this work $CrSi_2$ nanosize islands were grown by reactive deposition epitaxy (RDE) of Cr on n-type Si(111) and covered with 100 nm of epitaxial silicon. The structures with buried $CrSi_2$ NCs are investigated by atomic force microscopy (AFM), ultraviolet photoelectron spectroscopy (UPS), transmission electron microscopy (TEM), and optical reflectance spectroscopy to determine the atomic and electronic structure. Rutherford backscattering (RBS) was used to measure the distribution of Cr. Deep level transient spectroscopy (DLTS) was applied to identify the electrically active defects.

2. Experimental details

The $CrSi_2$ NCs and the silicon cap layer were grown in an ultra high vacuum (UHV) chamber without breaking the vacuum. The optical properties of the samples were studied in a Varian UHV chamber with a base pressure of 2×10^{-10} Torr equipped with Auger electron spectroscopy (AES) and DOS [5] facilities.

Samples were cut from n-type 7.5 Ω cm Si(111) substrates. The silicon cleaning procedure was as follows: annealing at 700 °C for 4–5 h, cooling for 12 h, and flashes at 1250 °C (five times). Surface purity was controlled by AES. RDE of Cr was carried out on a 500 °C substrate from a Ta tube. The Cr deposition rate was about 0.04 nm min^{-1} controlled by a quartz sensor.

A silicon cap layer was grown by MBE at 750 °C with a deposition rate of 3–4 nm min^{-1}. The thickness of the cap was 100 nm. The influence of the deposited Cr thickness (0.1–1.5 nm) on the growth and on the properties of Si(111)/$CrSi_2$-NCs/Si structures was studied. To study the nucleation of $CrSi_2$ islands and the influence of substrate temperature on the coalescence and coagulation of the NCs, samples were grown with Cr thicknesses of 0.1, 0.3 and 0.6 nm without a silicon cap layer and additional annealing (750 °C, 2 min) was applied. A sample with 0.3 nm of Cr deposited at 500 °C and covered by a 50 nm epitaxial silicon layer grown at 750 °C was prepared for UPS measurements.

Optical reflectance spectra after Si overgrowth were investigated using an automatic spectrophotometer Hitachi H-3010 with an integrated sphere and MDR-3 spectrophotometer (LOMO, Sankt-Petersburg, Russia) in the photon energy range 0.55–6.2 eV.

The morphology was studied by AFM (Solver P47) in semicontact mode using a 10 nm radius tip. A Philips CM 20 transmission electron microscope at 200 keV was used to measure planar and cross-sectional specimens, and a JEOL 3010 high-resolution transmission electron microscope (HRTEM) equipped with an energy filtering attachment (EFTEM) was also applied. For the TEM study, the specimens were thinned by our standard procedure, involving cutting with a diamond saw, embedding the pieces into a special titanium disc, mechanical grinding and polishing, and finally ion beam milling. Ar^+ ions of 10 keV energy were used until perforation, followed by low-energy (3 keV) milling to minimize surface damage [6]. Both cross-sectional and plan-view geometry specimens were prepared and studied.

The point defects were studied by DLTS in Schottky junctions prepared by the evaporation of 0.4×0.4 mm^2 gold dots onto the silicon cap and by applying Ga Ohmic contacts on

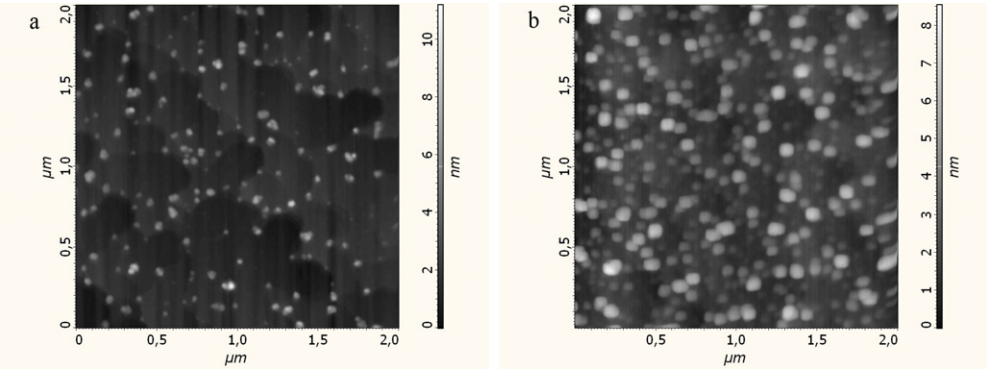

Figure 1. AFM images of samples prepared by RDE onto 500°C Si(111) 7×7 substrates of different thicknesses of Cr: (a)—0.1 nm; (b)—0.6 nm. Right-hand axes show a color scale of the height in nanometers.

the substrate. The distribution of Cr in silicon was measured by RBS using a 2 MeV $^4He^+$ analyzing ion beam with a spot size of $\sim 0.5 \times 0.5$ mm^2. Backscattered He^+ ions were detected at scattering angles of $\theta = 165°$ and 97°.

3. Results

The samples prepared by RDE of Cr with thicknesses of 0.1, 0.3 and 0.6 nm without a Si cap layer were measured by AFM to characterize the transition of $CrSi_2$ epitaxial layer growth to nanoisland formation. The surface morphology measured by AFM after RDE deposition of 0.1 nm of Cr is shown in figure 1(a). The islands are flat with a density of (3–4) $\times$ 10^9 cm^{-2}, a height of 2–4 nm, and lateral sizes of 20–40 nm. Only part of them coagulates in groups of two to four islands without coalescence. The surface is mostly covered by faceted islands. An atomically clean silicon surface between the NCs is shown by the LEED Si(111) 7 $\times$ 7 pattern with increased background. This background in LEED is due to the partial disordering of the silicon surface between $CrSi_2$ islands. After RDE of 0.6 nm of Cr and additional annealing, the measured AFM image is shown in figure 1(b). The majority of the islands have lateral sizes of 50–60 nm, but some of them have a smaller size and height. The island density is 7 $\times$ 10^9 cm^{-2}, double that shown in figure 1(a). The increase in the island density indicates that secondary nucleation occurs during Cr deposition, in parallel to the growth of the islands. Increasing the Cr thickness above a few monolayers and applying short annealing at 750 °C, the density of the nanoislands is increased without forming a continuous silicide layer. In the annealed samples, about 50% of the silicon surface is covered by nanoislands.

Since the maximal intensity LEED pattern and minimal background was observed at 750 °C [4], the silicon cap over the $CrSi_2$ NCs was grown at this temperature. The LEED Si(111) 7 × 7 pattern was preserved after the growth of a silicon overlayer in all samples, which corresponds to monolithic Si(111) with embedded $CrSi_2$ NCs. The morphology of the silicon cap layer was measured by AFM. The AFM images in figures 2(a)–(c) show the morphology of samples prepared by RDE of 0.1 nm, 0.6 nm, and 1.5 nm of Cr, respectively. The right-hand axes show a color scale of the height in nanometers. There are two characteristic formations: nanopit (NP) and nanohill (NH). The NPs have a lateral size of 20–25 nm and a depth of about 6–8 nm. The NHs typically have lateral sizes of 30–35 nm anda height of 3–4 nm. A higher-magnification 3D AFM image of the 0.6 nm Cr deposition sample is shown in figure 2(d). Some of the NHs are grown within an NP, as shown in figure 2(e).

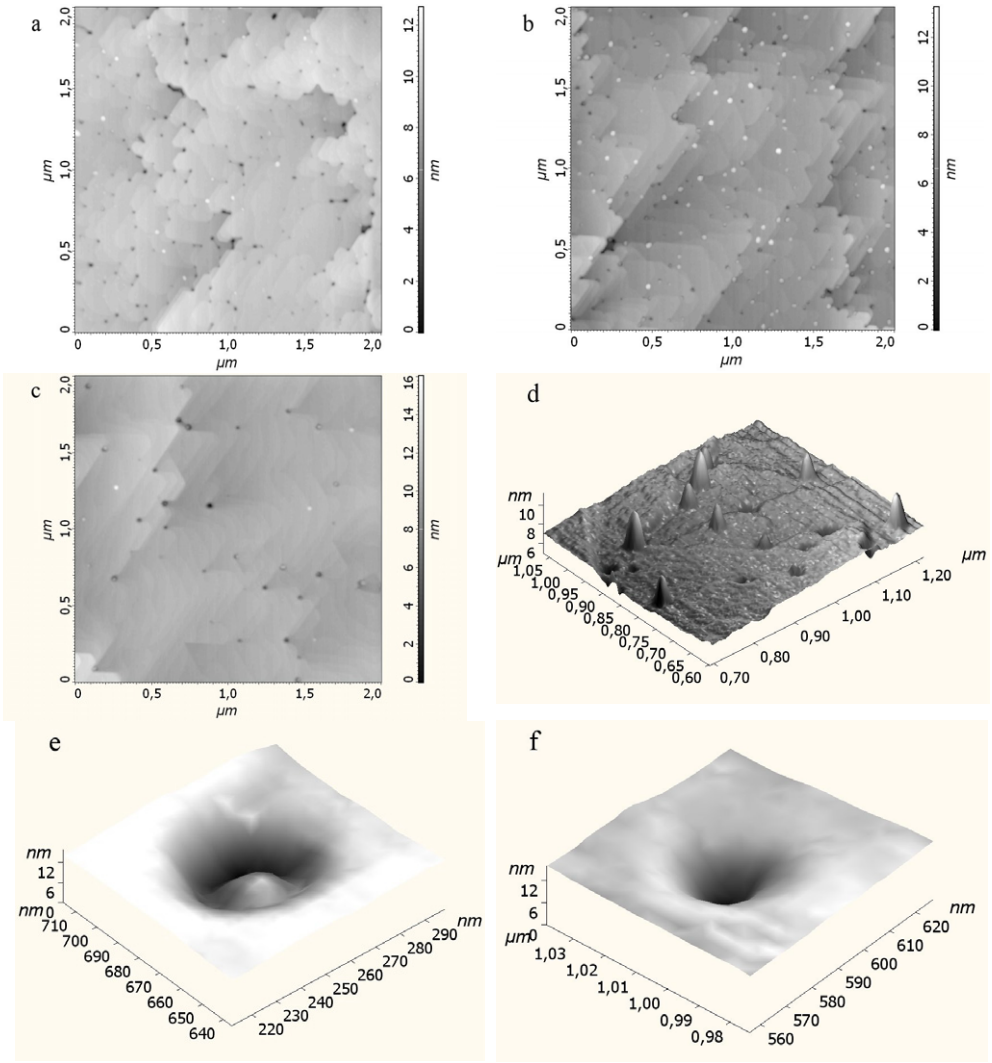

Figure 2. AFM images of Si(111)/$CrSi_2$ NCs/Si structures prepared by RDE of different thicknesses of Cr: (a) 0.1 nm; (b) 0.6 nm; (c) 1.5 nm; (d) 3D image of the 0.6 nm Cr sample; (e) higher magnification of a nanohill grown in a nanopit (e), and of a nanopit (f) in the 1.5 nm Cr sample. Right-hand axes show a color scale of the height in nanometers.

The density and typical size of NPs and NHs in samples prepared by RDE of different thicknesses of Cr are given in table 1.

At small Cr thicknesses, NPs are nearly circular. By increasing the Cr thickness, more and more NHs are grown in an NP in nearly hexagonal form, as shown in figure 2(e). The top of the NHs is pyramidal but its size is comparable to the AFM tip radius, so the measured form is a convolution with the AFM tip geometry. NHs and NPs are also circular in thick Cr samples, as is shown in figures 2(d) and (f). It is not possible to distinguish crystalline phases by AFM, but it is apparent that the crystallization of silicon in NP and NH formation depends on the Cr content. The density of NHs is maximal in samples grown from 0.6 nm Cr, where it is approximately one half of the $CrSi_2$ nanoisland density observed after the deposition of Cr

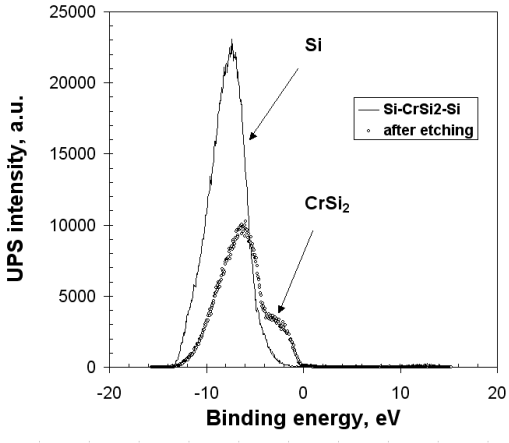

Figure 3. UPS intensity versus the binding energy for Si(111)/$CrSi_2$ NCs/Si heterostructure before (line) and after (circles) ion etching the silicon cap.

Table 1. Density, typical size, and the area covered by nanopits (NP) and nanohills (NH) measured by AFM and amplitude of the 1.8 eV peak in the ORS of samples containing $CrSi_2$ NCs prepared by RDE of different thicknesses of Cr.

Cr thickness (nm)	0.1	0.3	0.6	1.0	1.5
NP density (1 cm^{-2})	4.7×10^9	2.5×10^9	1.4×10^9	1.4×10^9	8×10^8
NP size (nm)	25	20	25	35	20
Area covered by NPs (%)	2.31	0.79	0.69	1.35	0.25
NH density (1 cm^{-2})	4×10^8	6×10^8	3×10^9	1.2×10^9	5×10^8
NH size (nm)	30	30	35	30	38
Area covered by NHs (%)	0.28	0.43	2.88	0.85	0.57
1.8 eV peak amplitude	0	0	2	1.8	3

and additional annealing (figure 1(b)). At Cr thicknesses higher than 0.6 nm, both the NH and NP densities decrease.

After the growth of a silicon cap layer over RDE of 0.3 nm of Cr, the UPS was measured. In the cap layer, only the signal of the silicon valence band appeared, as shown by the line in figure 3. After ion etching the silicon cap layer, the $CrSi_2$ valence band appeared, as shown by the empty circles in figure 3. The state density on the Fermi level equals zero, indicating that the NCs are in the semiconductor phase. This proves that the $CrSi_2$ NCs are conserved in a silicon lattice after silicon epitaxial growth at 750 °C, and that the $CrSi_2$ phase does not appear on the epitaxial silicon surface measured by UPS.

Comparison of the reflectance spectra of the grown NC layers with the spectra of a $CrSi_2$ epitaxial film [7] has shown a peak at 1.8 eV, which exists in the $CrSi_2$ epitaxial films as a strong shoulder. In the structures that were grown, it is seen as a separate peak in figure 4. In the 0.1 and 0.3 nm thick Cr samples, this peak does not appear. The 1.8 eV peak corresponds to 3D $CrSi_2$ NC segregation near the silicon surface. This proves that the 3D $CrSi_2$ phase does not appear on the surface in a significant amount in 0.1–0.3 nm Cr samples, in accordance with UPS.

Planar and cross sectional TEM investigations were used to determine the distribution of the NCs. The planar view bright field TEM image of the thinned edge of the 0.1 nm Cr sample is shown in figure 5(a). It indirectly shows the depth distribution of $CrSi_2$ NCs, since near the

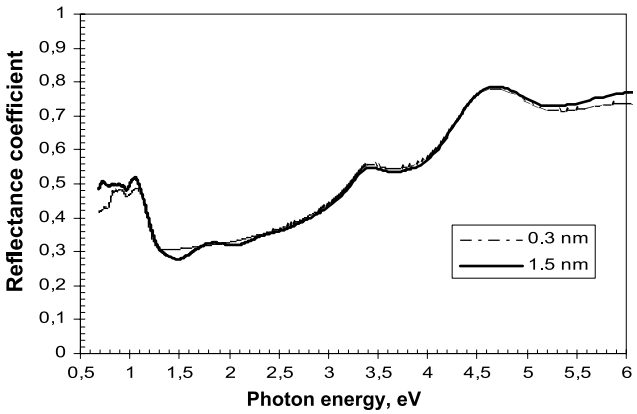

Figure 4. Optical reflectance spectra of two Si(111)/$CrSi_2$ NCs/Si samples with Cr thicknesses of 0.3 and 1.5 nm. At a photon energy below 1.2 eV, the contribution of multiple reflections in the silicon substrate is observed.

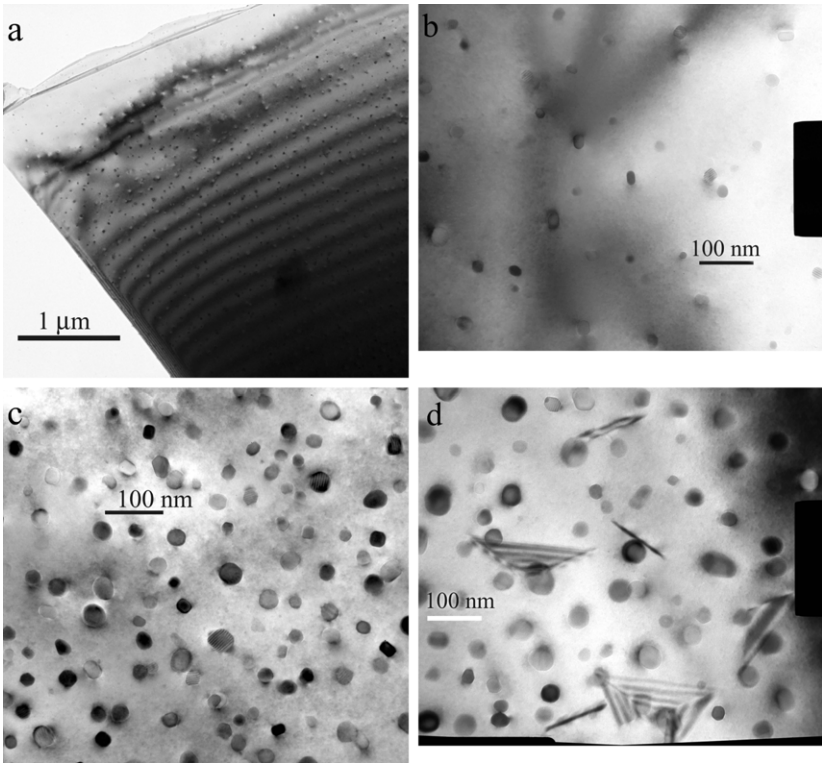

Figure 5. Planar-view bright-field TEM images of samples prepared by RDE of different thicknesses of Cr: ((a), (b)) 0.1 nm in two different magnifications; (c) 0.6 nm and (d) 1.5 nm.

thinned specimen edge (close to the top of the silicon layer) the density of NCs decreases. It also shows that the size of the NCs near the surface is smaller.

In figure 5(b), a larger-magnification image of the 0.1 nm Cr sample is shown. The density of the NCs is 6×10^9 cm^{-2}. A TEM image of the 0.6 nm Cr sample is shown in figure 5(c).

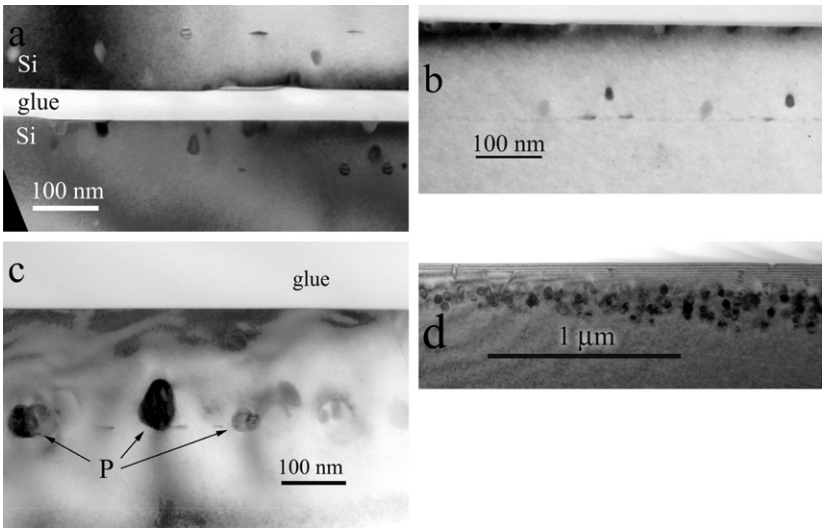

Figure 6. Cross-sectional TEM images of samples prepared by RDE at 500 °C of different thicknesses of Cr: (a) 0.1 nm; (b) 0,6 nm; (c) and (d) 1.5 nm.

The density of NCs is 2×10^{10} cm^{-2}. Their sizes are in the 20–40 nm range. A TEM image of the 1.5 nm Cr sample is shown in figure 5(d). The concentration of the NCs is 1.3×10^{10} cm^{-2}. The NCs are large and stacking faults are clearly visible, showing that the defect concentration is increasing in thick Cr deposited samples.

The cross-sectional TEM (XTEM) images of the 0.1 nm, 0.6 nm, and 1.5 nm Cr samples are shown in figures 6(a)–(c), respectively. The images show that, from 0.1 nm Cr, most of the NCs appear near the surface, while in the 0.6 nm Cr sample they are partly near the Si surface and partly near the deposition depth. In the 1.5 nm Cr sample, most of the NCs are localized around the deposition depth. In figure 6(d), a lower-magnification image of the 1.5 nm Cr sample is shown, where the scatter of the NC depth is apparent. It is remarkable that a dashed-line pattern appears in the XTEM image in the 0.1 and 0.6 nm Cr samples at the Cr deposition depth, indicating that some of the $CrSi_2$ islands are stabilized in two-dimensional (2D) form. The cross-sectional and planar-view TEMs show that most of the flat $CrSi_2$ nanoislands are transformed into 3D spherical NCs during growth of the silicon cap. This transformation is more effective in thicker Cr layer samples.

The distribution of the Cr was measured by EFTEM. The Cr is localized in the 3D NCs. The thin 'dashed-line' feature visible in the XTEM images of figure 6 at the Cr deposition depth are not seen in the EFTEM image. An XTEM image of the sample prepared by RDE of 1.5 nm Cr is shown in figure 7(a). A Cr map of the same area measured by cross-sectional EFTEM is shown in figure 7(b).

The depth distribution of the NCs in EFTEM is analogous to the XTEM; the Cr is present in all 3D NCs. In the 1.5 nm Cr sample, most of the NCs are about 130 nm below the surface, but some of them are shifted toward the surface. The HRTEM image of an NC in the 1.5 nm Cr sample is shown in figure 8. This shows that the $CrSi_2$ NC has hexagonal phase ($a = 0.4428$ nm, $c = 0.6369$ nm), epitaxially aligned to the Si(111) spacing ($d = 0.3135$ nm). The lattice constant in the c direction is, to a good approximation, double that of the Si lattice; the misfit is 1.5%. The truncated-sphere form is typical for large NCs in the 1.5 nm Cr sample, with the flat face located at the deposition depth. In the 0.1 and 0.6 nm Cr samples, the

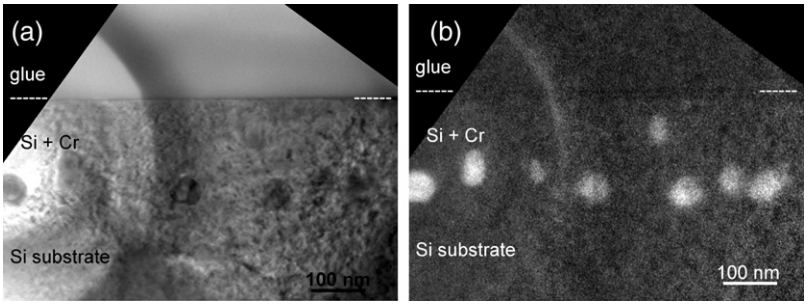

Figure 7. Transmission electron micrograph (a) and Cr elemental map (b) of a cross-sectional sample with 1.5 nm of Cr, showing the depth distribution of Cr–Si precipitates. Dashed lines indicate the sample surface. The bright circular region on the left is due to contamination by the focused electron beam.

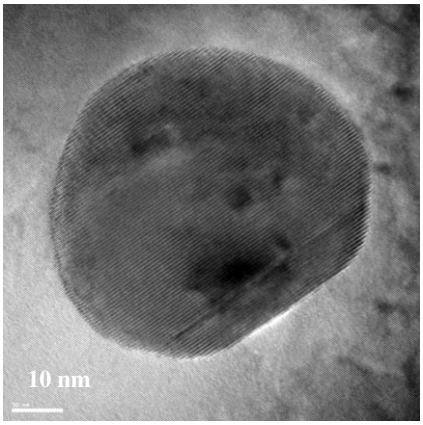

Figure 8. HRTEM image of a hexagonal phase $CrSi_2$ NC aligned to the Si(111) lattice spacing in the 1.5 nm Cr sample.

crystalline phase of the NCs with the faceted plane in the [111] direction is also hexagonal. These hexagonal NCs are nucleated near the deposition depth. The NCs near the surface are smaller and have a different crystalline structure. Further TEM experiments are needed to identify the crystalline phase of these NCs. It does not seem to be any of the identified bulk Si–Cr phases.

The electrical characteristics were measured in Schottky junctions. The current–voltage (I–V) characteristics of the junctions by RDE of different thicknesses of Cr are shown in figure 9. The Cr thickness, in units of angstroms, are used to mark the curves.

The series resistance dominates the I–V curves in all samples. The resistance is about 1 kΩ at 300 K in the 0.1 nm Cr sample, which increases to 56 kΩ at 77 K. The capacitance–voltage (C–V) characteristics of the junctions are shown in figure 10. At the applied Schottky junction area, a capacitance of about 130 pF belongs to a 100 nm depleted layer thickness, i.e. to the nominal cap thickness. The capacitance of the junctions with 0.1–0.6 nm of Cr is below 50 pF. This shows that the depleted layer edge is deep in the substrate. The large series resistance does not allow the evaluation of the doping concentration from the C–V characteristics. This may be due to the large concentration of states in the $CrSi_2$ NCs. The region around the NCs is also emptied of free carriers in the 1.0 and 1.5 Cr deposited samples, but the depleted layer edge

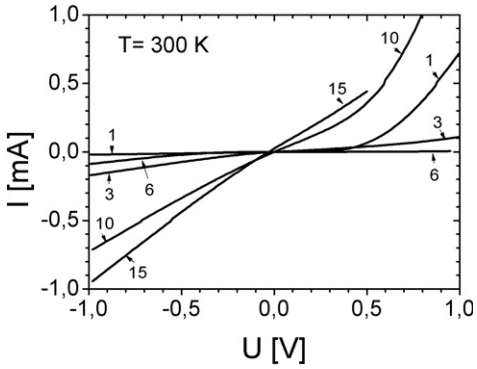

Figure 9. I–V characteristics of the Schottky junctions on $Si/CrSi_2$ NC/Si structures prepared by RDE of different thicknesses of Cr. The Cr thicknesses, in units of angstroms, mark the curves.

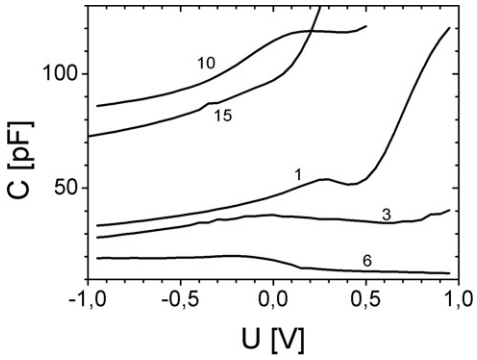

Figure 10. C–V characteristics of the Schottky junctions on $Si/CrSi_2$ NC/Si structures prepared by RDE of different thicknesses of Cr. The thickness of the Cr, in units of angstroms, mark the curves.

in these sample approaches the NC plane. To check the conductivity type of the cap layer, Ga Ohmic contacts were also prepared on the cap. The I–V measurement of these junctions shows that the NCs develop a potential barrier in the silicon. In these samples the C–V curves are symmetric, and their capacitance depends on the Ohmic contact area. This indicates that the top silicon layer has a high resistivity. Since the doping level in the cap layer is low, it can be emptied by the electrical field of the charged NCs. The measured I–V and C–V characteristics suggest that the silicon cap conductivity type changes from p to n at a Cr thickness of 0.6 nm. For better analysis of electrical characteristics, a higher doping level in the cap is required.

The DLTS spectra measured in the 0.1 nm Cr sample at repetition rates of 25 Hz (▼), 250 Hz (▲), and 2500 Hz (●) are shown in figure 11. The spectra were taken at a reverse bias of -1 V, and with 20 μs, 0 V filling pulses.

The energy position of the defect calculated from the DLTS Arrhenius plot is about 0.25 eV, appropriate for the Cr–B complex at $E_v + 0.23$ eV in p-type silicon and for the Cr level at $E_c - 0.27$ eV in n-type silicon [8]. The concentration of the defects calculated from the DLTS amplitude is in the 10^{13} cm^{-3} range. However, this can be an underestimation, since the capacitance strongly depends on the temperature and it does not satisfy the basic assumptions for accurate DLTS analysis. The double peak may be a result of the large series resistance, since the excitation pulses cannot relax during the DLTS repetition cycle. The large series

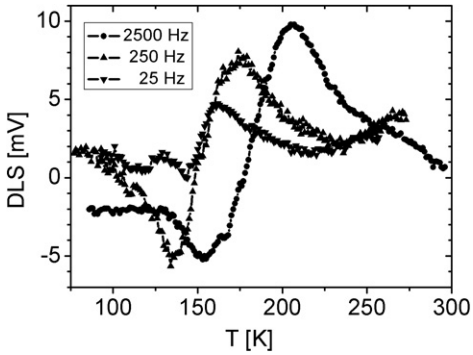

Figure 11. DLTS spectra of a Schottky junction on Si/$CrSi_2$ NCs/Si grown by RDE of 0.1 nm Cr measured at repetition rates of 25 Hz (▼), 250 Hz (▲), and 2500 Hz (●). The spectra were taken at a reverse bias of −1 V, with a 20 μs, 0 V filling pulse. Arrhenius plots gives activation energies at $E_v + 250$ meV and at $E_c - 270$ meV.

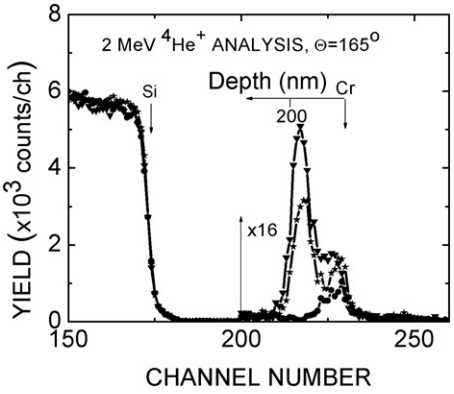

Figure 12. RBS spectra of the Si(111)/$CrSi_2$ NCs/Si structures prepared by RDE of 0.1(●), 0.6 (*) and 1.5 nm (▼) Cr. The spectra were taken with a 2 MeV He^+ beam at a random angle of incidence, and detected at 165°.

resistance can be explained by Cr point defects compensating the cap layer doping around the deposition depth. It is remarkable that the concentration found in DLTS is small compared to the density of NCs found in planar-view TEM (about 10^{10} cm^{-2} in the 10^{-5} cm cap silicon). This indicates that the DLTS defect level attributed to Cr may be directly related to the $CrSi_2$ NCs, not to the isolated Cr atoms. The defects cannot be characterized by DLTS in the thicker Cr RDE samples, since the applied pulses do not change the occupancy of the defects. C–V and I–V measurements are sensitive to illumination, showing that the resistance of the cap layer is reduced by illumination. This also proves that the silicon cap is good quality; it is not dominated by recombination centers. Further experiments in samples with higher doping in the cap layer are needed to better identify the point defects.

RBS measures a large concentration of Cr in the cap layer, as show in figure 12.

RBS spectra of the Si(111)/$CrSi_2$ NCs/Si structures prepared by RDE of 0.1(●), 0.6 (*) and 1.5 nm (▼) Cr at an observation angle of 165° are shown in figure 12. At this observation angle the Cr signal is well separated from that of Si. The total amounts of Cr are 1.1×10^{16} cm^{-2}, 7.8×10^{15} cm^{-2}, and 1.8×10^{15} cm^{-2}, which correspond to 1.3 nm, 0.9 nm, and 0.2 nm Cr for samples with thicknesses of nominally 1.5 nm, 0.6 nm, and 0.1 nm Cr, respectively. The

evaluation of RBS spectra was performed by the RBX program [9]. The resolution of the Cr depth distribution determination by RBS with these measuring parameters is about 35 nm. The Cr peak at the sample surface is marked by a down-arrow below the 'Cr' label. The spectra show that most of the Cr in the 0.1 nm Cr sample diffuse near to the surface during growth of the Si cap layer. The other Cr peak is centered at around 170 nm depth in the 0.6 and 1.5 nm Cr deposited samples. In the 0.6 nm Cr RDE sample, the peak at the sample surface is slightly increased compared to the 0.1 nm Cr sample, while in the 1.5 nm Cr the excess Cr remains near the deposition depth and the Cr content near the surface does not increase further. In the 0.6 nm Cr sample, about 60% of the Cr is localized near the Cr deposition depth, while in the 1.5 nm Cr sample about 75% of the Cr is localized near the Cr deposition depth.

4. Discussion

The AFM results show that the presence of NCs does modify the morphology of the silicon cap layer, resulting in NPs and NHs. The NP density decreases with the amount of Cr deposited. The NH density increases with Cr thickness up to 0.6 nm, and above this it decreases. TEM shows that the density of NCs is maximal for 0.6 nm of Cr. From Cr layers below 0.6 nm, an increasing number of NCs are grown near the surface. This indicates that during growth of the Si cap at 750 °C a few monolayers of Cr diffuse towards the surface. We assume that the diffusion of Cr takes place in the form of small-size silicide NCs below the surface. NPs are a result of the deficit of Si atoms due to the growth of 3D NCs below the surface. HRTEM shows that the NPs are due to NCs grown near the surface. The crystalline phase of the NCs near the deposition depth is hexagonal $CrSi_2$. Some of the NCs near the surface are of a different crystalline phase, which is not identified yet. The generation of the NPs and NHs and their size and density on a silicon surface depends on the silicon cap growth rate and on the amount of Cr NCs near the surface. At small Cr thicknesses (0.3 nm and less) $CrSi_2$ NCs are small and are not stabilized in 3D $CrSi_2$ NCs during RDE deposition. The small silicide NCs diffuse during silicon deposition at 750 °C and are transformed into 3D NCs near the Si surface. This forms a large amount of NPs on the silicon cap. Some of the NPs show the top of the $CrSi_2$ NCs and have hexagonal facets, which is manifested as NH in the NP. At Cr thicknesses of 0.6–1.5 nm, large $CrSi_2$ islands with lateral sizes of 50–60 nm are formed. These large NCs are stable during the silicon cap growth. EFTEM shows that the Cr is accumulated in the 3D NCs. We suppose that in the thick Cr samples the large 3D $CrSi_2$ NCs collect the Cr from the small $CrSi_2$ NCs. More efficient collection of Cr in thick Cr samples can be due to longer annealing at 500 °C during RDE, since a constant Cr deposition rate was applied. In thick Cr RDE samples, the NCs are stable during growth of the silicon cap. This shows that a critical size of NCs is required for their stabilization. The large, immobile NCs nucleated at the deposition depth decrease the Cr concentration on the epitaxial growth front. The decrease in Cr concentration on the surface improves the silicon growth and results in a decrease in the NP and NH densities on the surface. It is known that Cr has a tendency above 700 °C to diffuse toward the surface [10], so we suppose that the silicon has a continuous high Cr concentration ($>10^{21}$ cm^{-3} range) at the growth front during growth of the cap layer. This explains the nucleation and growth of $CrSi_2$ NCs far from the original Cr deposition plane, as observed by TEM, and also explains the NPs and NHs observed by AFM on the surface. The detailed process depends on nucleation of the silicon epitaxy on the $CrSi_2$ NCs and on the transformation kinetics of the 2D nanoisland and small NCs to large 3D hexagonal $CrSi_2$ NCs. A more precise description of the process requires further study by using a different RDE growth rate and applying annealing before the silicon cap growth to stabilize the $CrSi_2$ NCs.

The Cr concentration measured by RBS is appropriate for the amount of the deposited Cr. RBS results show that a few monolayers of Cr diffuse to the surface during growth of

the silicon cap, and above a few monolayers Cr mostly reacts with Si near to the deposition depth. Electrical characteristics indicate that only a small part of the Cr atoms appear in electrically active point defects. Photocurrent and photocapacitance shows a low concentration of recombination centers in the cap layer. The defect concentration calculated from the DLTS signal amplitude is small compared to the density of NCs measured by TEM. The energy positions of the defects determined by DLTS are in agreement with the Cr point defect positions described in the literature. This can be a result of a silicon layer around the Cr deposition depth compensated by Cr point defects, however the defects measured by DLTS may be related to the $CrSi_2$ NCs. In that case, the positive and negative peak DLTS Arrhenius plots give the valence- and conduction-band discontinuities of the $CrSi_2$ NCs relative to the appropriate silicon bands. Further experiments with a more highly doped cap layer are needed for better identification of the electrically active defects.

5. Conclusions

Monolithic Si(111)/$CrSi_2$ NCs/Si(111) structures with buried $CrSi_2$ NCs were grown and investigated. It was shown that the semiconductor properties of $CrSi_2$ NCs are preserved in the silicon matrix independently of the deposited Cr thickness (0.1–1.5 nm). The large NCs nucleated near the deposition depth have been identified as hexagonal phase $CrSi_2$ aligned to the silicon (111) lattice spacing. Further experiments are needed to identify the crystalline structure of the NCs near the surface. A Cr concentration in the 10^{21} cm^{-3} range was measured by RBS in the silicon cap layer. The point defects measured by DLTS are at about 0.25 eV above the valence band and 0.27 eV below the conduction band of silicon. These defect energy positions are appropriate for the Cr level observed in n- and p-type silicon in the literature. DLTS has shown a low defect concentration in the silicon cap. Since the concentration measured by DLTS is small not only compared to the concentration of Cr measured by RBS but even compared to the density of NCs measured by TEM, the observed DLTS signal may be related directly to the $CrSi_2$ NCs. The difference between the bulk and TEM results can be explained by the volume investigated by RBS and DLTS being several order of magnitude larger. The defects increase the resistivity of the epitaxial silicon layer by reducing the electron concentration. The observed large redistribution of Cr shows that, to improve the distribution of the NCs, the growth temperature at the initial stage of the silicon cap growth has to be reduced and/or some annealing process has to be applied before the silicon cap epitaxy to stabilize the hexagonal $CrSi_2$ NCs at the deposition depth.

Acknowledgments

The authors thank Mr E A Chusovitin (Institute for Automation and Control Processes of the Far Eastern Branch of the Russian Academy of Sciences (FEB RAS)) for the AFM images. The work was performed with financial support from FEB RAS grant no. 06-02-P1-001, the Russian Foundation of Basic Research (RFBR) grant no. 07-02-00958_a, and a program between the Russian Academy of Sciences and the Hungarian Academy of Sciences (2005–2007, project no. 22).

References

[1] Borisenko V E (ed) 2000 *Semiconducting Silicides* (*Springer Series in Materials Science* vol 39) (New York: Springer)

[2] Wetzel P, Pirri C, Peruchetti J C, Bolmont D and Gewinner G 1988 *Solid State Commun.* **65** 1217–20

[3] Galkin N G, Velitchko T V, Skripka S V and Khrustalev A B 1996 *Thin Solid Films* **280** 211–20
[4] Galkin N G, Goroshko D L, Dotsenko S A and Turchin T V 2007 *J. Nanosci. Nanotechnol.* at press doi:10.1166/jnn.2007.A076
Galkin N G, Goroshko D L, Turchin T V, Dotsenko S A, Cherednichenko A I and Davydov V A 2006 *Asia-Pacific Conf. on Semiconductor Silicides (APAC-SILICIDE 2006) (Kyoto University, Kyoto, July 2006)* pp 123–4 Extended abstracts
[5] Dotsenko S A, Galkin N G, Gouralnik A S and Koval L V 2005 *e-J. Surf. Sci. Nanotechnol.* **3** 113
[6] Barna A, Pécz B and Menyhard M 1998 *Ultramicroscopy* **70** 161–71
[7] Galkin N G, Maslov A M, Konchenko A V, Kaverina I G and Gouralnik A S 1998 *Opt. Spectrosc.* **85** 601–6
[8] Mishra K 1996 *Appl. Phys. Lett.* **68** 3281–3
[9] Kótai E 1996 *Proc. 14th Int. Conf. on Appl. Accelerators in Res. Ind. (Denton, TX, Nov. 1997)* ed J L Duggan and I L Morgan (New York: AIP) p 631
[10] Zhang P, Steven F, Vanfleet R, Neelakantan R, Klimov M, Zhou D and Chow L 2004 *J. Appl. Phys.* **96** 1053–8